ChemCatChem

Research Article
doi.org/10.1002/cctc.202501164

Chemistry Europe
European Chemical Societies Publishing

www.chemcatchem.org

Catalytic Activity of Water-Dispersed Palladium Nanoparticles with Different Sizes and Shapes in the Semihydrogenation of Alkynes

Niklas Kost[+],[a] Florian Lehmann[+],[b] Rui Guo,[a] Kateryna Loza,[a] Marc Heggen,[c] Thomas Seidensticker,*[b] and Matthias Epple*[a]

Palladium nanoparticles of different sizes and shapes dispersed in water, stabilized by either polyvinylpyrrolidone or glutathione, were studied in both monophasic and biphasic alkyne hydrogenation reactions at 50 bar hydrogen pressure. Spherical nanoparticles of 2 and 5 nm diameter as well as cubic nanoparticles of 18 and 28 nm edge length were investigated. Structural changes in the particles before and after the catalytic reactions were assessed with respect to agglomeration and particle size. The particle size had the strongest effect on the catalytic efficiency, i.e., spherical nanoparticles of 5 nm were the most active and spherical nanoparticles of 2 nm were the least active. The nanocubes had intermediate catalytic activities. Semihydrogenation occurred within minutes at low palladium loadings. The highest turnover frequencies of about 183,000 h^{-1} were achieved with 5 nm palladium nanoparticles. Mass transport limitations constrained the reaction rates in aqueous biphasic systems with larger nanoparticles.

1. Introduction

Metallic nanomaterials have found many applications in catalysis due to their remarkable properties compared to the bulk phases. This is mainly due to their high specific surface area.[1–3] Palladium nanoparticles are especially important in heterogeneous catalysis, e.g. for hydrogenation[4,5] and cross-coupling reactions.[6] Ultrasmall nanoparticles, i.e., smaller than 3 nm in diameter, have a particularly high surface area with good colloidal stability.[2,3] Therefore, they behave like homogeneous catalysts while simultaneously acting as heterogeneous catalysts. This dual nature bridges the gap between homogeneous and heterogeneous catalysis, combining the high activity, selectivity, and mild reaction conditions of homogeneous catalysts with the easy catalyst retrieval (e.g., by membrane filtration) of heterogeneous systems. This opens up new avenues for more efficient and sustainable catalytic processes.[7,8]

Various larger palladium nanoparticles have been investigated in catalysis, with studies exploring the influence of particle size, shape, and stabilizing ligands, particularly in alkyne hydrogenation, which is a key reaction in fine chemistry and polymer production.[7] Palladium is the preferred metal for alkyne hydrogenation, although it is usually applied in supported form.[7] Both nanoparticle size and shape have been shown to affect the catalytic performance, usually ascribed to differences of the active sites on the particle surface.[9] Planar crystal faces were identified as the most important for hydrogenation catalysis. Crystal edges and corners lead to selective alkyne-to-alkene hydrogenation, but at high conversions, they also catalyze the hydrogenation of alkene to the corresponding alkane.[9] The catalytic behavior of palladium nanoparticles is influenced not only by their shape and size, which determine turnover frequency (TOF) and selectivity, but also by their capping agents, which can alter their surface properties and restrict the access of a substrate to the metal surface.[10] For example, the polymer poly(N-vinylpyrrolidone) (PVP), which is frequently used as capping agent for nanoparticles[9,11–14] initially inhibits the catalytic activity by covering the active surface sites, but gradually desorbs to expose more catalytically active parts of the surface.[15–17] On the other hand, glutathione (GSH) is a smaller capping agent that has a strong stabilizing effect on metal particles of different size and shape.[18–20] Therefore, it is another promising choice to coat catalytically active palladium nanoparticles.[4]

Ultrasmall palladium nanoparticles have been synthesized but rarely tested for their catalytic activity.[2,4,14,18,21–23] Usually, palladium nanoparticles larger than 5 nm were used in alkyne

[a] N. Kost[+], R. Guo, K. Loza, M. Epple
Inorganic Chemistry and Centre of Nanointegration Duisburg-Essen (CENIDE), University of Duisburg-Essen, Universitaetsstr. 5-7 45117, Essen, Germany
E-mail: matthias.epple@uni-due.de

[b] F. Lehmann[+], T. Seidensticker
Department for Biochemical and Chemical Engineering, Laboratory for Industrial Chemistry, TU Dortmund University, Emil-Figge-Str. 66 44227, Dortmund, Germany
E-mail: thomas.seidensticker@tu-dortmund.de

[c] M. Heggen
Ernst Ruska Centre for Microscopy and Spectroscopy with Electrons, Forschungszentrum Jülich 52428, Jülich, Germany

[+] Both authors share first authorship.

Supporting information for this article is available on the WWW under https://doi.org/10.1002/cctc.202501164

hydrogenation.[24] It appears to be an attractive option to use ultrasmall palladium nanoparticles with their very high specific surface area as catalysts to reduce the amount of necessary palladium. Only two reports have addressed the hydrogenation of alkynes or alkenes by ultrasmall colloidally dispersed nanoparticles so far.[4,24]

The hydrogenation of alkynes with palladium nanoparticles is usually carried out at low hydrogen pressure (1 to 4 bar) in liquid single-phase systems,[9–11,24–28] with the only exception of Telkar et al. who used 24 bar.[29] Hydrogen pressures above 24 bar were never applied together with dispersed catalytically active nanoparticles. Furthermore, palladium nanoparticles have not yet been applied in the aqueous biphasic hydrogenation of alkynes.

Closing this gap in knowledge, we report here on the catalytic activity of palladium nanoparticles of well-defined and uniform size, shape, and surface functionalization in high-pressure hydrogenation, focusing on their high specific surface area and resource-efficient material use. We compare their catalytic activity in alkyne hydrogenation in a monophasic as well as in a biphasic system. Besides the assessment of the catalytic efficiency, we isolated the particles after the reaction and analyzed them by transmission electron microscopy to shed light on possible changes that occurred during the catalytic reaction.

2. Experimental Section

All chemicals were obtained with a purity of at least 98% and used without further purification (see Supporting Information).

For the preparation of spherical ultrasmall palladium nanoparticles (2 nm),[2] disodium tetrachloropalladate (Na_2PdCl_4, 60 mg, 1 eq.) was dissolved in 230 mL water in a 500 mL round bottom flask. Glutathione (GSH, 128 mg, 2 eq.) dissolved in 10 mL cold water was added. The solution changed its color from light-yellow to orange within 2 min. After 10 min, a freshly prepared solution of sodium borohydride (46 mg, 6 eq.) in 10 mL cold degassed water was quickly added. The color of the solution rapidly changed to brown–black. After 12 h, the glutathione-coated ultrasmall black palladium nanoparticles were isolated by spin filtration (5 kDa SpinX UF 20 centrifuge filters; 45 min, 4000 rpm). Finally, the nanoparticles were washed several times with 15 mL water each by spin filtration. In an earlier study, the number of GSH ligands on a similar type of palladium nanoparticles was determined to 117 GSH ligands on each 1.8 nm particle.[2] For the larger palladium nanoparticles, the number of ligands on the surface is not known because NMR spectroscopy is not applicable in this case.[30]

PVP-coated spherical palladium nanoparticles (5 nm) were prepared according to a published procedure.[14] The ligand exchange of PVP to GSH in 5 nm nanoparticles was carried out by dispersing the palladium nanoparticles (10.6 mg, 100 µmol palladium content) in 190 mL water. 1 g glutathione dispersed in 10 mL water was added and the dispersion was stirred for 24 h. The particles were isolated by spin filtration in 30 kDa SpinX UF 20 centrifuge filters (45 min, 4,000 rpm).

PVP-coated palladium nanocubes (18 nm) were prepared according to a published procedure.[12,13] PVP-coated palladium nanocubes (28 nm) were prepared as follows: 18 nm PVP-coated palladium nanocubes were used as seeds for the on-growth of palladium. This involved the dissolution/dispersion of PVP_{55} (55 kDa, 150 mg), ascorbic acid (90 mg), potassium bromide (450 mg), and palladium nanocubes (18 nm, 1.8 mg) in a 50 mL round-bottom flask in 12 mL water, followed by vigorous shaking. Subsequently, the mixture was heated to 40 °C for 10 min. Then, a solution of Na_2PdCl_4 (0.02 M in 5 mL water) was added, and the mixture was stirred at 40 °C for 24 h. Then, the reaction mixture was quenched with an ice bath. The particles were isolated by centrifugation (14,200 rpm; 21190 g; 30 min) and washed twice with water. For the ligand exchange of PVP to GSH, 18 or 28 nm Pd-PVP nanocubes (5 mL, 2.5 mg Pd) were dispersed in 2.5 mL water, respectively, and mixed with glutathione (200 mg, dissolved in 2.5 mL water). The reaction mixtures were stirred for 12 h. The nanoparticles were isolated by centrifugation (14,200 rpm; 21,190 g; 30 min) and washed twice with water.

Transmission electron microscopy (TEM) was performed with an FEI TEM 80–300 instrument with an accelerating voltage of 300 kV.[31] The nanoparticle dispersions were deposited onto copper grids that were coated with an ultrathin amorphous carbon film and dried in air. The size of the 2 nm nanoparticles was determined by the program ANTEMA.[32] The size of the 5 nm nanoparticles was determined manually with the program ImageJ.[33] Scanning electron microscopy (SEM) was performed with an Apreo S LoVac instrument (Thermo Fisher Scientific, USA) with nanoparticles prepared as for TEM. The size of the nanocubes was determined manually with the program ImageJ.[33]

Differential centrifugal sedimentation was carried out with a CPS Instruments DC 24,000 disc centrifuge, operating at 24,000 rpm and 29,000 g. A density gradient was obtained by overlaying with two sucrose solutions of 8 and 24 wt%, respectively. Dodecane (0.5 mL) was added to the top layer to prevent evaporation. Prior to each measurement, a calibration standard of polyvinylchloride (PVC) with a defined hydrodynamic diameter of 263 nm dispersed in water was measured. The volume of the added aqueous nanoparticle dispersion was 100 µL. The hydrodynamic diameter of the nanoparticles was calculated with the density of elemental palladium (12.023 g cm^{-3}). Hydrodynamic particle size distributions were also determined by dynamic light scattering (DLS) with a Malvern Zetasizer Nano ZS ZEN 3600 instrument with nanoparticles in aqueous dispersion.

For the ICP analysis, the sample was dried at 150 °C and then digested with 8 mL 67% HNO_3 in a CEM Mars 6 microwave instrument. Afterwards, the sample was dispersed in 3 mL deionized water and measured in an ICP-OES instrument (Plasma Quant PQ9000 Elite, Analytik Jena).

For hydrogenation at 1 atm, the concentrated nanoparticle dispersions were ultrasonicated for 5 min. Then, an aliquot was diluted to the desired content of palladium with deionized water, followed by stirring for 5 min. Reactions at 1 atm hydrogen were conducted in round bottom flasks with stopcock that were flushed with argon under stirring at 1,400 rpm for at least 5 min after the diluted catalyst solution had been added. A constant hydrogen supply was realized with a hydrogen balloon. To exchange argon by hydrogen, the flask was flushed with one complete balloon without stirring. Next, the nanoparticles were preformed for 10 min under stirring at 1,400 rpm. The substrate was added with a syringe, any possible overpressure was released, and a new balloon was attached with subsequent short flushing. For reactions at elevated temperatures, the reaction time was started after the desired temperature was reached. Aliquots were taken with a syringe and rapidly quenched.

A 120 mL stainless steel reactor was sealed, flushed with argon, and evacuated for high-pressure reactions. This was repeated three times. The catalyst dispersion was introduced into the reactor in argon counterflow; subsequently, the substrate container was charged by applying argon counterflow. Afterwards, the reactor was pressurized to 50 bar hydrogen under constant stirring at 1,500 rpm. After reaching a constant pressure, a preforming time of 10 min was allowed before the substrate was added to the preformed cata-

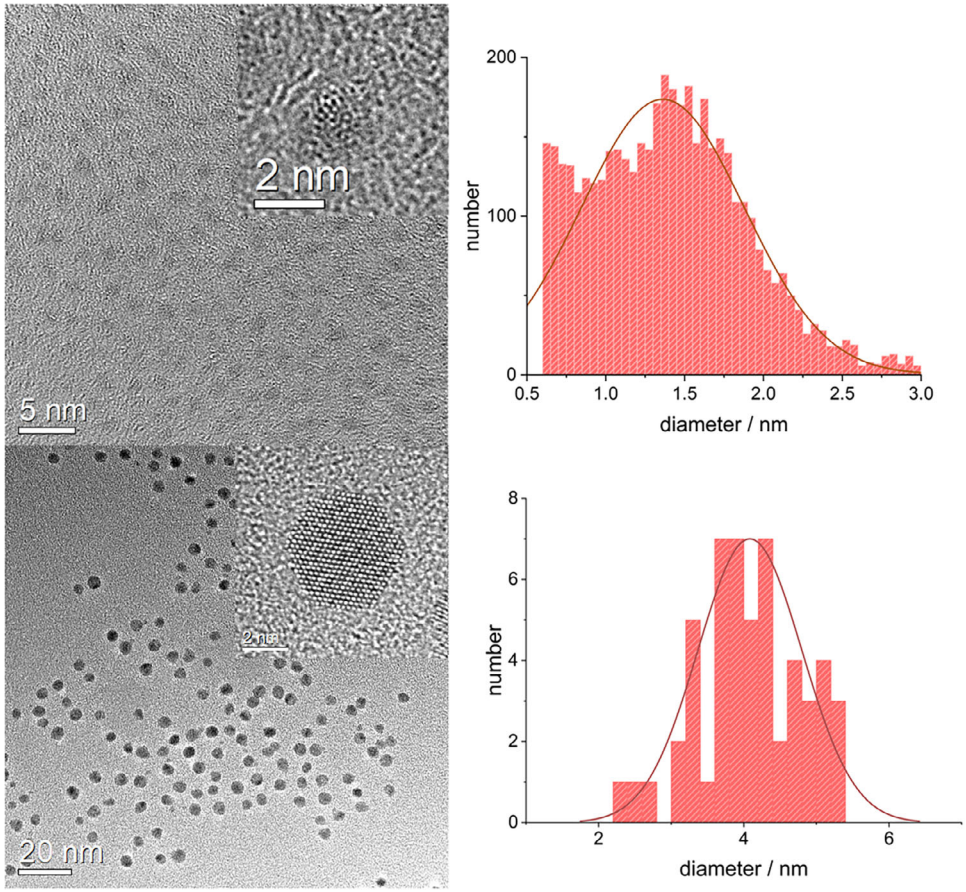

Figure 1. Top: HRTEM images of GSH-coated ultrasmall palladium nanoparticles (2 nm), together with the particle size distribution (>2000 particles were analyzed, average diameter: 1.5 ± 0.4 nm). **Bottom**: HRTEM images of larger PVP-coated palladium nanoparticles (5 nm), together with the particle size distribution (50 particles were analysed; average diameter: 4.4 ± 0.7 nm).

lyst solution. During the reaction, aliquots were taken and rapidly quenched with liquid N_2-frozen glassware. In the hydrogenation experiment with the Lindlar catalyst, the catalyst was placed inside the reactor prior to sealing, and no water was added.

All samples were analyzed by GC analysis with an FID detector and *tert*-butanol or o-xylene as external standards for quantitative analysis. For the biphasic hydrogenation, additional GC-MS-EI and NMR analyses were performed to exclude the formation of positional isomers.

3. Results and Discussion

3.1. Nanoparticle Characterization

Different types of palladium nanoparticles were prepared as potential catalysts: three types of spherical nanoparticles, i.e., 2 nm GSH-coated nanoparticles (denoted as ultrasmall nanoparticles in the following) and 5 nm PVP- or GSH-coated nanoparticles. The affinity of PVP to the palladium surface is weaker than that of the thiol-containing ligand GSH, a fact that may influence the catalytic activity.[4]

The diameter of the metal core was determined by high-resolution transmission electron microscopy (HRTEM; Figure 1). The average diameter of the ultrasmall nanoparticles was 1.5 ± 0.4 nm. The larger PVP-stabilized spherical nanoparticles

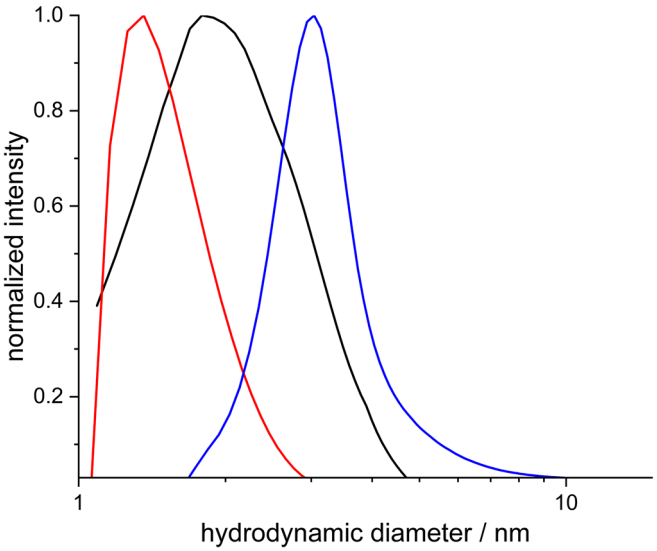

Figure 2. Differential centrifugal sedimentation (DCS) of GSH-coated ultrasmall palladium nanoparticles (2 nm, **red**), PVP-coated larger palladium nanoparticles (5 nm, **blue**), and GSH-coated larger palladium nanoparticles (5 nm, **black**), dispersed in water. The average diameter of the ultrasmall nanoparticles was 1.5 ± 0.4 nm. The average diameter of the PVP-coated larger nanoparticles was 3.1 ± 0.6 nm. The average diameter of the GSH-coated larger nanoparticles was 2.1 ± 0.9 nm.

(5 nm) had an average diameter of 4.4 ± 0.7 nm. Note the crystallographic well-developed faces of the 5 nm nanoparticles.

Differential centrifugal sedimentation (DCS) gave the hydrodynamic diameter of water-dispersed nanoparticles (Figure 2). Note that ultrasmall particles appear smaller in DCS because their effective density is lower than that of the metal core due to the surrounding ligand shell.[34]

A complementary method is dynamic light scattering (DLS), which was applicable only to the 5 nm nanoparticles because the ultrasmall nanoparticles do not scatter the light (Figure 3).

Two different sizes of palladium nanocubes were prepared with edge lengths of 18 and 28 nm, respectively, coated either with PVP or with GSH. The HRTEM images of the smaller nanocubes showed uniform cubes with slightly rounded corners. The HRTEM images of the larger nanocubes showed uniform cubes with minor surface defects (Figure 4). Scanning electron microscopy gave average edge lengths of 18 ± 2 and 28 ± 2 nm, respectively (Figure 5). The 18 nm cubes are mostly regular but the 28 nm cubes have concave faces. Although this is difficult to assess in a quantitative way, it indicates that the exposed crystallographic faces are different for both types of cubes which may also influence their catalytic activity.

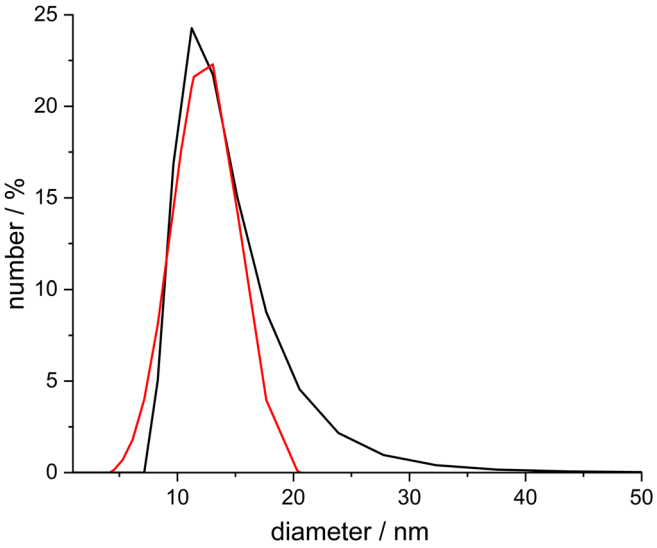

Figure 3. Dynamic light scattering (DLS) of PVP-coated larger palladium nanoparticles (5 nm), dispersed in water. The average diameter was 12 ± 3 nm (**black**). DLS of GSH-coated larger palladium nanoparticles (5 nm), dispersed in water. The average diameter was 7 ± 1 nm (**red**).

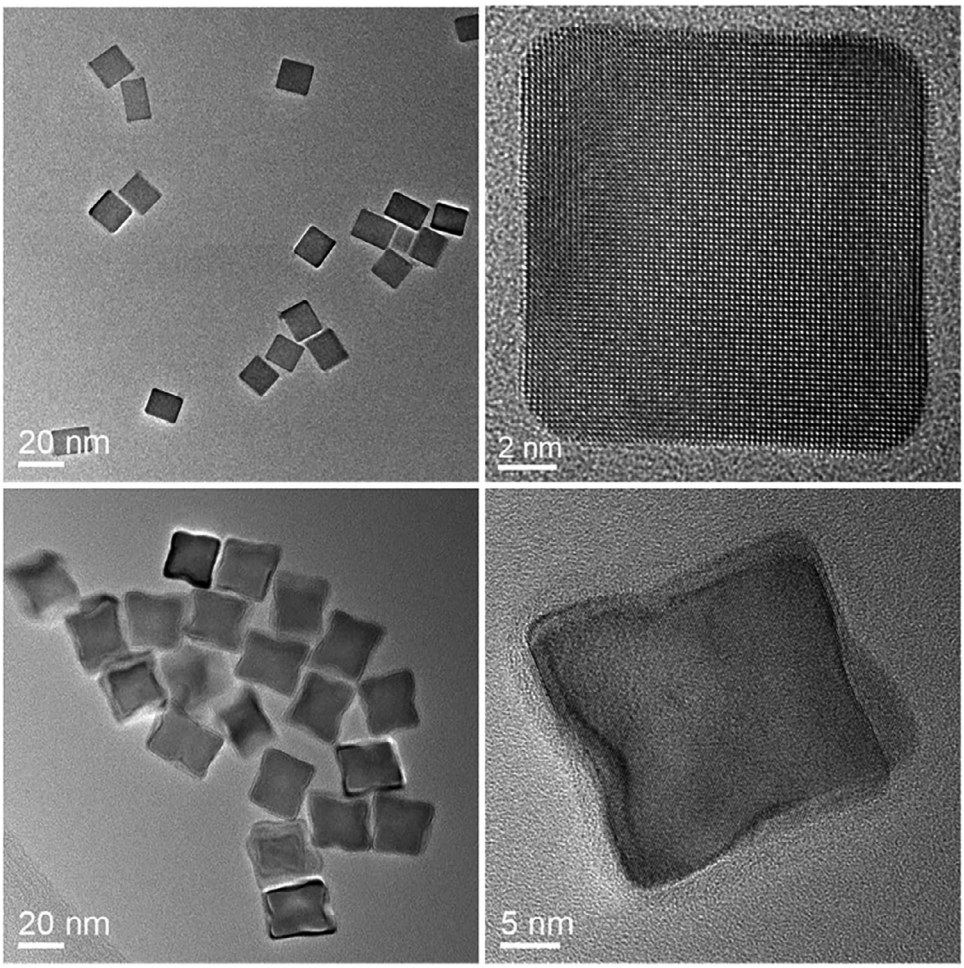

Figure 4. Top: HRTEM image of smaller PVP-coated palladium nanocubes (18 nm). **Bottom**: HRTEM image of the larger PVP-coated palladium nanocubes (28 nm).

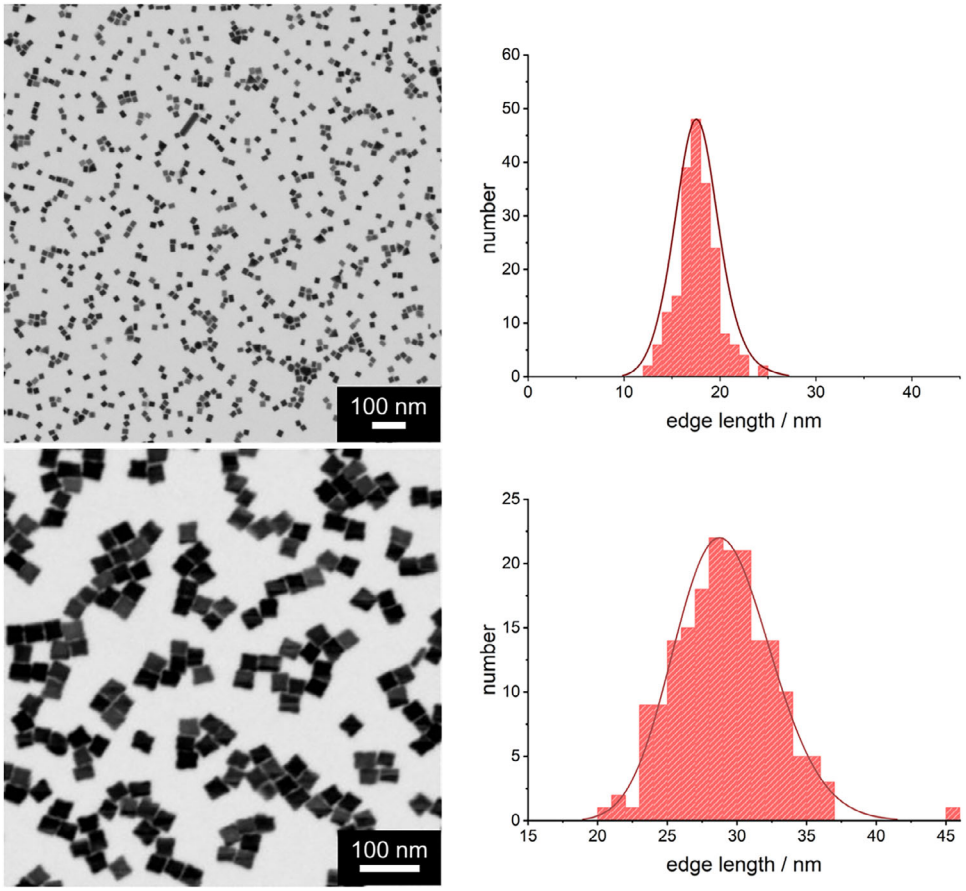

Figure 5. Top: Scanning electron microscopy of smaller PVP-coated palladium nanocubes (18 nm), together with their particle size distribution (203 particles were analysed, average edge length: 18 ± 2 nm). **Bottom**: Scanning electron microscopy of larger PVP-coated palladium nanocubes (28 nm), together with their particle size distribution (185 particles were analysed, average edge length: 28 ± 2 nm).

DCS (Figure 6) and DLS (Figure 7) gave the hydrodynamic diameters of the water-dispersed nanocubes, both with GSH- and PVP-coating. The higher hydrodynamic diameter by DLS in comparison to the core diameter by TEM indicates a moderate degree of agglomeration. Table 1 summarizes all size characterization data of the nanoparticles.

After the detailed characterization of the particles, they were tested in the semihydrogenation reaction of alkynes. Figure 8 illustrates the relative dimensions of the molecular substrates 2-methyl-3-butyne-2-ol **1** and 1-octyne **2** in comparison to the palladium nanoparticles. The substrate 1-octyne has a similar size as the ultrasmall palladium nanoparticles.

3.2. Hydrogenation of 2-Methyl-3-butyne-2-ol (Monophasic)

First, the GSH-coated ultrasmall nanoparticles were applied in the monophasic semihydrogenation of 2-methyl-3-butyne-2-ol (**1**, Scheme 1) to identify suitable reaction conditions.

Initially, a standard approach was used, conducting the experiment at 1 atm hydrogen pressure with variable catalyst loadings and at variable temperature. Catalyst loadings as low as 0.016 mol% Pd were found to be catalytically active. However, the maximum conversion of **1** never exceeded 45%, regardless

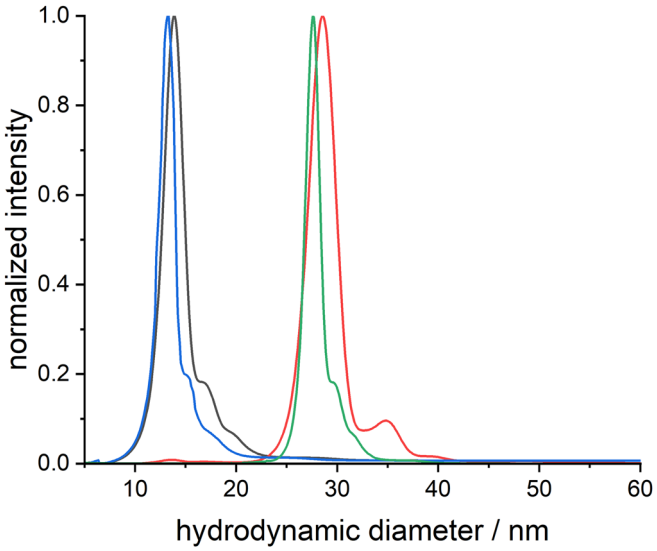

Figure 6. Differential centrifugal sedimentation (DCS) of smaller (18 nm) and larger (28 nm) palladium nanocubes, coated with either PVP or GSH. The GSH-coated nanoparticles had hydrodynamic diameters of 13 nm (**blue**) and 26 nm (**green**). The PVP-coated palladium nanoparticles had hydrodynamic diameters of 15 nm (**black**) and 28 nm (**red**), respectively.

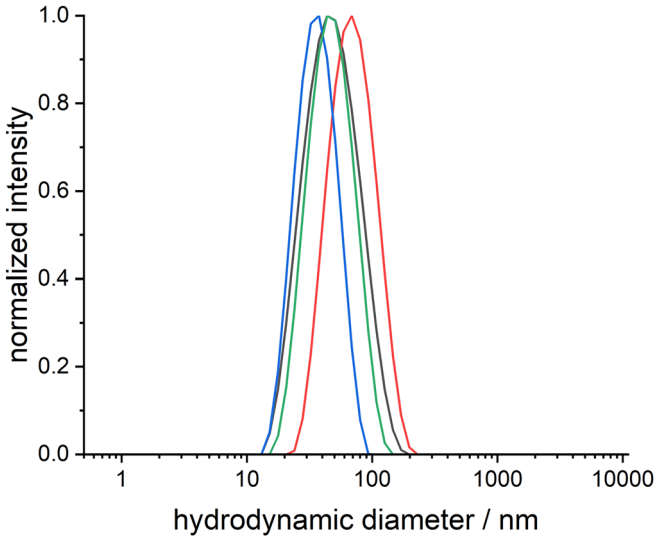

Figure 7. Dynamic light scattering (DLS) data of smaller (18 nm) and larger (28 nm) palladium nanocubes, coated with either PVP or GSH. The PVP-coated nanocubes had hydrodynamic diameters of 47 nm (**black**) and 68 nm (**red**), respectively. The GSH-coated nanocubes had hydrodynamic diameters of 35 nm (**blue**) and 47 nm (**green**), respectively.

of the catalyst concentration and the temperature (see Figures S1 and S2). Furthermore, TEM analysis of the ultrasmall palladium nanoparticles recovered after the hydrogenation reaction of **1** at 1 atm H_2, 25 °C and 0.016 mol% Pd showed strongly aggregated nanoparticles (Figure S3). Therefore, the hydrogen pressure was increased to 50 bar to achieve a full substrate conversion. We found that at all investigated catalyst loadings, the hydrogenation of **1**–**3** at 50 bar and room temperature occurred within a few minutes (Figure 9). Notably, a selectivity of 84% toward the desired alkenol **3** was observed when approaching full conversion. Over-hydrogenation to *tert*-amyl alcohol **4** and dimer formation occurred only in minor amounts in that case. As expected, alkynes were hydrogenated significantly faster than alkenes.[9]

At full conversion, a temperature maximum was reached, which decreased during over-hydrogenation (Figure 10). This can be explained by the different reaction enthalpies associated with the conversions from alkyne to alkene and from alkene to alkane of the same species,[35] coupled with different rates of the individual reaction steps, and heat exchange across the reactor wall. This was also reported by Brunet et al.[27] Thus, the reaction progress was monitored non-invasively by monitoring the temperature in the reactor. Aliquots were taken toward the end of the plateau phase for analysis. Taking into account the reaction rate and the selectivity, 0.016 mol% Pd was chosen as the catalyst loading for all further experiments. The selectivity at complete conversion ($X \geq 99\%$) is particularly relevant because it correlates with the maximum yield. This underscores the intrinsic selectivity of this catalyst configuration because over-hydrogenation is expected to become more prominent at an excess of alkenes over alkynes.[7,9,11]

Table 1. Characterization data of all palladium nanoparticles used for hydrogenation catalysis.

Coating	Shape	Particle Core Diameter or Edge Length by Electron Microscopy/nm	Hydrodynamic Diameter by DCS/nm	Hydrodynamic Diameter by DLS/nm
GSH	Spheres (2 nm)	1.5 ± 0.4	1.5 ± 0.4	–
GSH	Spheres (5 nm)	4.4 ± 0.7	2.1 ± 0.9	7 ± 1
GSH	Cubes (18 nm)	18 ± 2	13 ± 1	35 ± 4
GSH	Cubes (28 nm)	28 ± 2	26 ± 1	47 ± 5
PVP	Spheres (5 nm)	4.4 ± 0.7	3.1 ± 0.6	12 ± 3
PVP	Cubes (18 nm)	18 ± 2	15 ± 1	47 ± 5
PVP	Cubes (28 nm)	28 ± 2	28 ± 2	68 ± 7

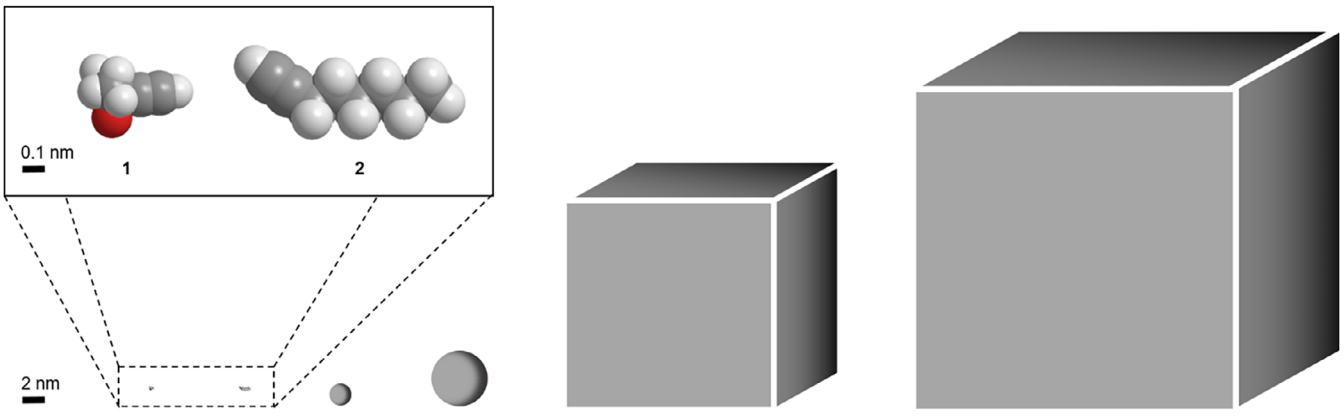

Figure 8. Schematic size comparison of the substrates (**1**: 2-methyl-3-butyne-2-ol, **2**: 1-octyne) with all palladium nanoparticles used for heterogeneous catalysis.

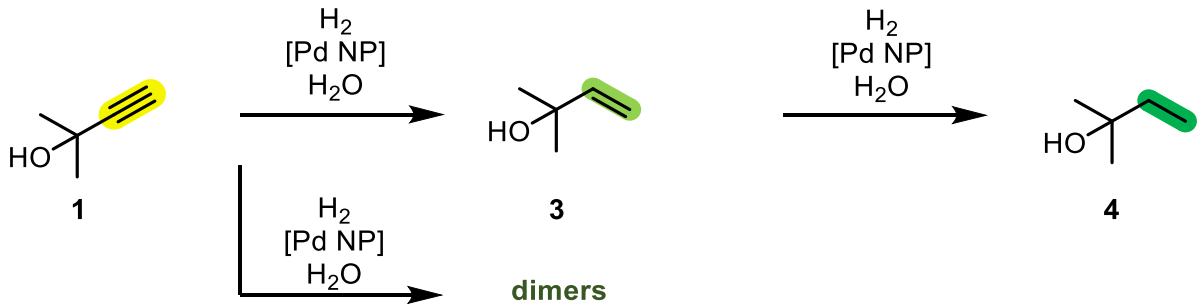

Scheme 1. Reaction network of the hydrogenation of 2-methyl-3-butyne-2-ol (**1**), catalyzed by palladium nanoparticles.

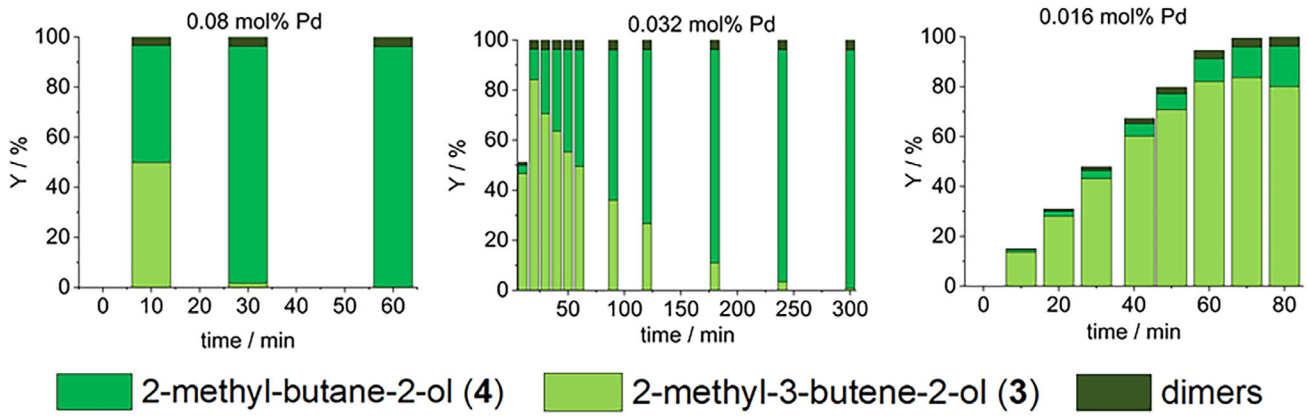

Figure 9. *Y*,*t*-plots of the hydrogenation of **1** at 50 bar H_2 catalyzed by GSH-coated ultrasmall palladium nanoparticles (2 nm) at different catalyst loadings. General conditions: $n_{substrate}$ = 50 mmol, p_{H2} = 50 bar, $f_{stirrer}$ = 1500 rpm, T_{start} = RT, V_{total} = 58.1 mL, $t_{preforming}$ = 10 min, semibatch conditions; **left**: c_{Pd} = 0.08 mol%, $w_{Pd,H2O}$ = 80 ppm; **center**: c_{Pd} = 0.032 mol%, $w_{Pd,H2O}$ = 32 ppm; **right**: c_{Pd} = 0.016 mol%, $w_{Pd,H2O}$ = 16 ppm.

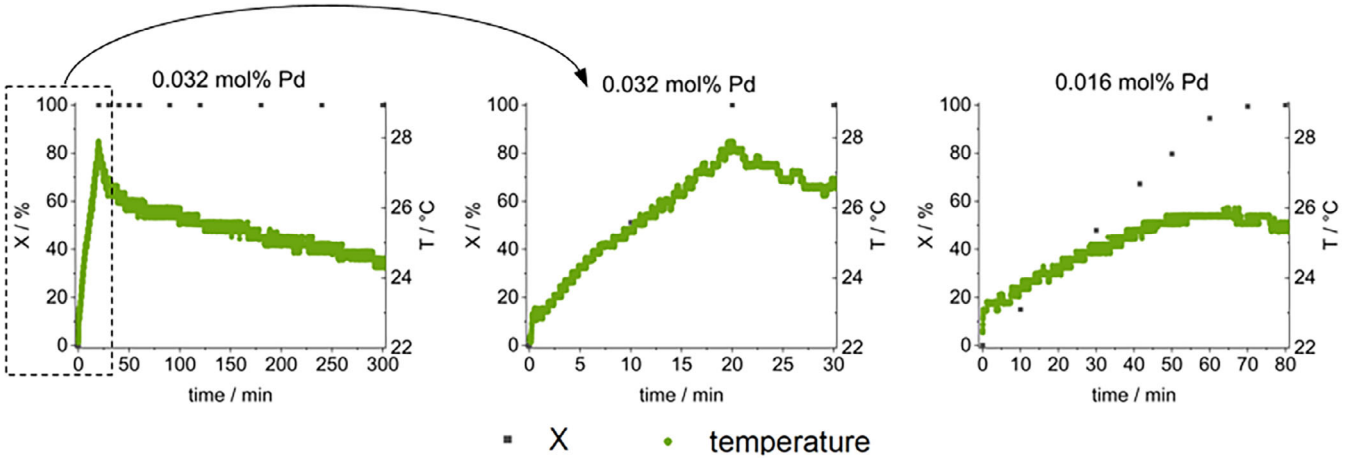

Figure 10. Development of reactor temperature and conversion during the hydrogenation of **1** at 50 bar H_2 with GSH-coated ultrasmall palladium nanoparticles (2 nm) at different catalyst loadings. General conditions: $n_{substrate}$ = 50 mmol, p_{H2} = 50 bar, $f_{stirrer}$ = 1500 rpm, T_{start} = RT, V_{total} = 58.1 mL, $t_{preforming}$ = 10 min, semibatch conditions; **left**: c_{Pd} = 0.032 mol%, $w_{Pd,H2O}$ = 32 ppm, **center**: enlarged section of the left image, **right**: c_{Pd} = 0.016 mol%, $w_{Pd,H2O}$ = 16 ppm.

Further monophasic hydrogenation experiments of **1** catalyzed by the other types of palladium nanoparticles were performed under the same conditions. The results are shown in Table 2.

The ultrasmall nanoparticles showed the lowest reaction rate (entry 2.1). Notably, a complete conversion was not achieved for the large GSH-coated nanocubes (entry 2.4), and the reaction significantly slowed down with time. The selectivity at full conversion was high in all cases, ranging from 76% to 88%. The 5 nm particles showed the highest reaction rate, regardless of the capping ligand (GSH or PVP, entries 2.2 and 2.5). ICP analysis gave very high recoveries for most types of palladium nanoparticles, suggesting that palladium remained well dispersed in the liquid phase. Only

Table 2. Overview of hydrogenation reactions of **1** (monophasic). Conditions: $n_{substrate}$ = 50 mmol, p_{H2} = 50 bar, $f_{stirrer}$ = 1500 rpm, c_{Pd} = 0.016 mol%, $T_{star\ t}$ = RT, $w_{Pd,H2O}$ = 16 ppm, V_{total} = 58.1 mL, $t_{preforming}$ = 10 min, semibatch conditions.

Entry	Coating	Shape	$d_{core/edge\ length,\ before}$ / nm	$d_{core/edge\ length,\ after}$/nm	S[a)]/%	$t_{T,max}$/s	TOF/h^{-1}	Pd Recovery[b)]/ppm
2.1	GSH	Spheres (2 nm)	1.5 ± 0.4	1.5 ± 0.3	84	3866–4061	4400	Full
2.2	GSH	Spheres (5 nm)	4.4 ± 0.7	3.6± 0.6	84	125–132	177000	Full
2.3	GSH	Cubes (18 nm)	18 ± 2	17 ± 2	88	634–684	27000	Full
2.4	GSH	Cubes (28 nm)	28 ± 2	26 ± 2	–[c)]	3812–4271[d)]	3000[d)]	10
2.5	PVP	Spheres (5 nm)	4.4 ± 0.7	3.4 ± 0.6	76	122–138	183000	Full
2.6	PVP	Cubes (18 nm)	18 ± 2	13 ± 2	88	2233–2307[d)]	4100[d)]	Full
2.7	PVP	Cubes (28 nm)	28 ± 2	24 ± 3	81	1402–1713	15000	4

[a)] At full conversion.
[b)] The theoretical recovery is 14.85 ppm Pd at maximum; "full" indicates values between 12–17 ppm.
[c)] Full conversion was not reached.
[d)] Could be even lower, see Supporting Information for details.

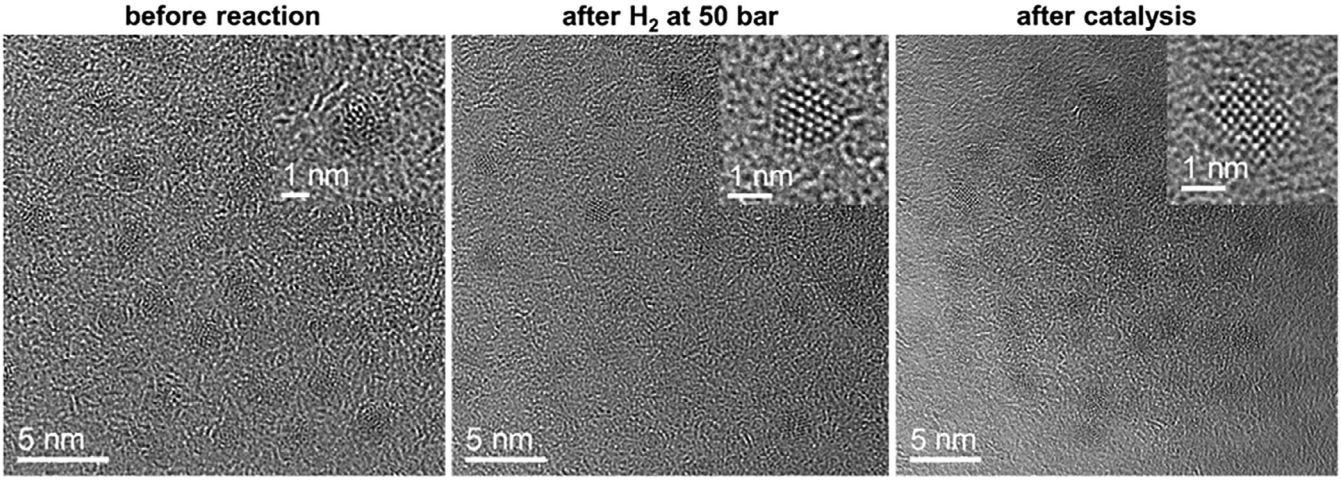

Figure 11. HRTEM images of ultrasmall GSH-coated palladium nanoparticles (2 nm) before the catalytic reaction (**left,** same as Figure 1), retrieved after stirring at 50 bar hydrogen pressure for 1 h (**center**), and retrieved after the hydrogenation reaction of **1** (**right**). Conditions: $n_{substrate}$ = 50 mmol, p_{H2} = 50 bar, $f_{stirrer}$ = 1500 rpm, c_{Pd} = 0.016 mol%, T_{start} = RT, $w_{Pd,H2O}$ = 16 ppm, V_{total} = 58.1 mL, $t_{preforming}$ = 10 min, semibatch conditions.

for PVP-coated 28 nm nanocubes, lower retrieval rates were observed.

A possible change of the shape and structure of the palladium nanoparticles during the hydrogenation of **1** at 50 bar hydrogen pressure was assessed by analyzing the retrieved nanoparticles by HRTEM (Figure 11). The crystallinity of the ultrasmall palladium particles had significantly increased due to the high hydrogen pressure (reduction of initially present PdO[2] to metallic palladium). This was confirmed by the treatment with hydrogen in the absence of the organic substrate. The particle core size remained unchanged. After retrieval, the ultrasmall nanoparticles were still well colloidally dispersed without noticeable agglomeration.

The corresponding HRTEM images of the larger GSH-coated palladium nanoparticles (5 nm) (entry 2.2) are shown in Figure 12. They had formed loose aggregates of approximately 30 nm in diameter, consisting of the original particles. In contrast, the nanocubes showed a pronounced aggregation but retained their original shape and size. Very similar results were obtained for PVP-stabilized nanoparticles (see Figure S4).

A benchmark hydrogenation experiment of **1** with a Lindlar catalyst at the same pressure, catalyst concentration, and initial temperature gave 83% selectivity after a reaction time of 33 min (Figure S6), i.e., an intermediate reaction rate with a selectivity comparable to the nanoparticles. Thus, the nanoparticles are a lead-free alternative to the Lindlar catalyst.

3.3. Hydrogenation of 1-Octyne (Biphasic)

Next, a biphasic hydrogenation reaction was tested (Figure 13). 1-Octyne **2** was used as water-immiscible substrate. In such a biphasic system, the initially water-dispersed particles may agglomerate and deposit on the walls of the reactor or on the phase interface. Furthermore, they may also leach from the aqueous phase into the product phase (Figure 14). Table 3 gives the results of the biphasic hydrogenation catalysis.

In the biphasic hydrogenation, the ultrasmall nanoparticles showed a significantly slower reaction rate compared to the

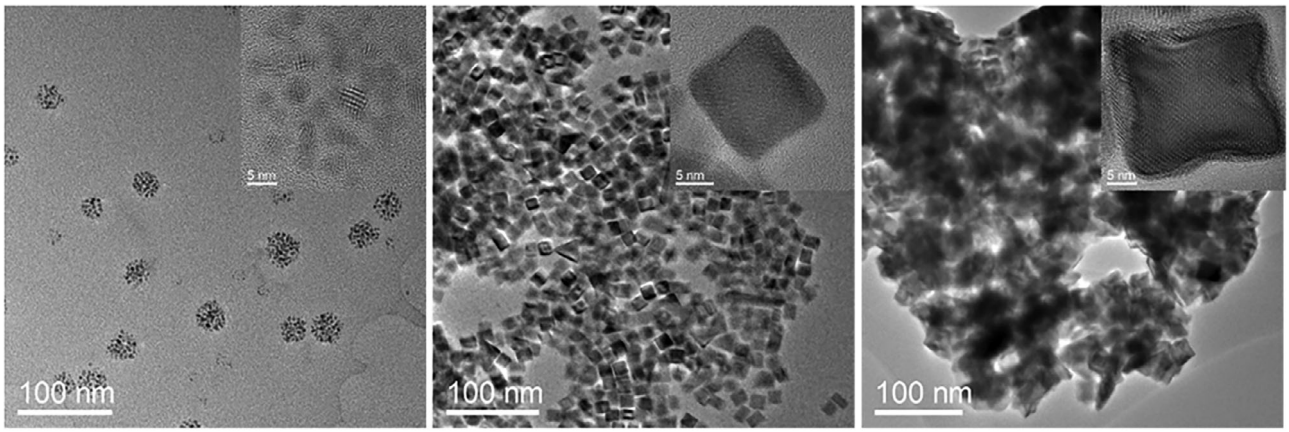

Figure 12. Overview and magnified HRTEM images of larger GSH-coated spherical palladium nanoparticles (5 nm) (**left**), smaller palladium nanocubes (18 nm) (**center**), and larger palladium nanocubes (28 nm) (**right**) after hydrogenation of **1** at 50 bar hydrogen pressure. Conditions: $n_{substrate}$ = 50 mmol, p_{H2} = 50 bar, $f_{stirrer}$ = 1500 rpm, c_{Pd} = 0.016 mol%, T_{start} = RT, $w_{Pd,H2O}$ = 16 ppm, V_{total} = 58.1 ml, $t_{preforming}$ = 10 min, semibatch conditions.

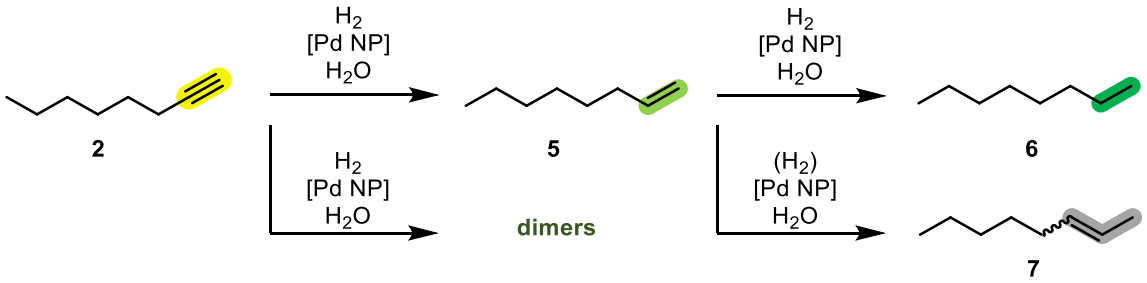

Figure 13. Reaction pathway of the biphasic hydrogenation of 1-octyne **2**, catalyzed by palladium nanoparticles.

Table 3. Results of hydrogenation reactions of **2** (biphasic). Conditions: $n_{substrate}$ = 50 mmol, p_{H2} = 50 bar, $f_{stirrer}$ = 1500 rpm, c_{Pd} = 0.016 mol%, T_{start} = RT, $w_{Pd,H2O}$ = 16 ppm, V_{total} = 60.6 mL, $t_{preforming}$ = 10 min, semibatch.

Entry	Coating	Shape	$d_{core/edge\ length,\ before}$/nm	$d_{core/edge\ length,\ after}$/nm	$S^{a)}$/%	$t_{T,max}$/s	TOF/h^{-1}	Pd leaching /%	Pd mass balance /%
3.1	GSH	Spheres (2 nm)	1.5 ± 0.4	1.6 ± 0.3	77	6800–8925	1000[b)]	2	+2
3.2	GSH	Spheres (5 nm)	4.4 ± 0.7	4.0 ± 0.5	51	594–781	21000	54	−40
3.3	GSH	Cubes (18 nm)	18 ± 2	16 ± 2	83	1283–1396	12000	1	−86
3.4	GSH	Cubes (28 nm)	28 ± 2	25 ± 2	88	1171–1465	16600	1	−80
3.5	PVP	Spheres (5 nm)	4.4 ± 0.7	3.2 ± 0.3	80	460–490	38000	7	−87
3.6	PVP	Cubes (18 nm)	18 ± 2	13 ± 2	77	1484–1780	13000	3	−66
3.7	PVP	Cubes (28 nm)	28 ± 2	20 ± 3	83	1485–1929	11000	3	−85

[a)] At full conversion.
[b)] Induction period within the regression time frame leading to imprecise linearization.

monophasic system (entry 3.1), requiring approximately 2.5 h for completion. Again, all other particles had a higher activity than the ultrasmall nanoparticles. The 5 nm nanoparticles gave the highest reaction rate (entries 3.2 and 3.5). However, this was accompanied by an increased rate of isomerization in the case of the GSH-coated particles, resulting in a decrease in selectivity to 51% (entry 3.2). All cubic particles (entries 3.3, 3.4, 3.6, and 3.7) had a similar reaction rate, possibly due to additional mass transport limitations during the biphasic reaction. In the same line, the 5 nm particles had a significantly lower reaction rate compared to the monophasic hydrogenation of **1**, suggesting mass transport limitation.

The loss of palladium was considerable for all particles except for the ultrasmall nanoparticles. The particles showed a pronounced accumulation of palladium at the phase interface, independent of their surface coating. Strong brown deposits were visually observed on the interface and also on the reactor surface.

The ultrasmall nanoparticles could not be recovered. The 5 nm GSH-coated nanoparticles (entry 3.2) were almost unchanged after hydrogenation in the two-phase system. The GSH-coated nanocubes (entries 3.3 and 3.4) were aggregated but mostly unchanged in size and shape (Figure 15). Similar results were obtained for PVP-coated particles (Figure S5).

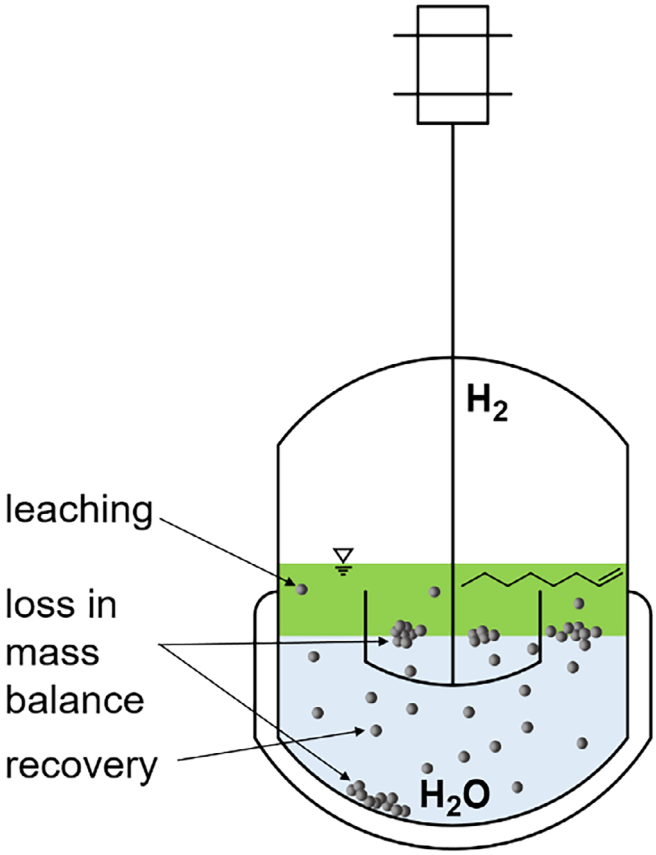

Figure 14. Possible processes that may occur with palladium nanoparticles in a biphasic oil-water system during catalysis.

Figure 16 depicts the relative reaction rates for both substrates and all types of palladium nanoparticles. In all cases, the 5 nm nanoparticles were the most efficient (shortest reaction time) and the 2 nm ultrasmall nanoparticles the least efficient (longest reaction time). The nanocubes gave intermediate reaction rates. For a possible explanation, we have computed the specific surface area of all catalysts samples used and also the number of accessible palladium atoms on the particle surface (Table 4). In relative terms and normalized to the catalyst mass, the palladium atoms on the particle surface are of the ratio 21:10:1.5:1 for spheres (2 nm):spheres (5 nm):cubes (18 nm):cubes (28 nm). This clearly illustrates that the catalytic efficiency is not proportional to the number of palladium atoms on the particle surface.

As the catalytic efficiency is not simply proportional to the specific surface area, other effects must be responsible. A possible explanation is that ultrasmall nanoparticles have a very rugged surface and therefore lack distinct crystallographically defined faces and therefore give lower reaction rates.[9,24] Furthermore, the lower reaction rates observed for the investigated nanocubes agree with simulations conducted by Crespo-Quesada et al. for nanoparticles of different size.[9] The surface coverage with the capping ligands (GSH and PVP) and the surface dynamics (desorption and re-adsorption) certainly have a major effect on the catalytic efficiency, like the turnover frequencies (TOF). Unfortunately, these data are not available for the initial particles. It can be underscored that all particles were thoroughly washed and purified by centrifugation, therefore, we can safely assume that the ligands are well attached to the nanoparticle surface before catalysis. However, it is not known what is happening with the ligand shell under catalytic conditions, e.g. in different solvents, at elevated temperature, and elevated hydrogen pressure. The fact that some particles were strongly agglomerated after the catalysis suggests that the ligand shell could be influenced. Unfortunately, there are no analytical methods available that can address this question in a quantitative way.

For transition-metal catalysts such as palladium, there is a strong ecological and economic incentive for facile separation, ideally in their active form, so that the catalysts can be reused after recovery. Biphasic systems have proven to be a useful concept for molecular catalysts, therefore, we aimed to transfer this concept to the present catalyst system. However, when introducing a second phase, distribution phenom-

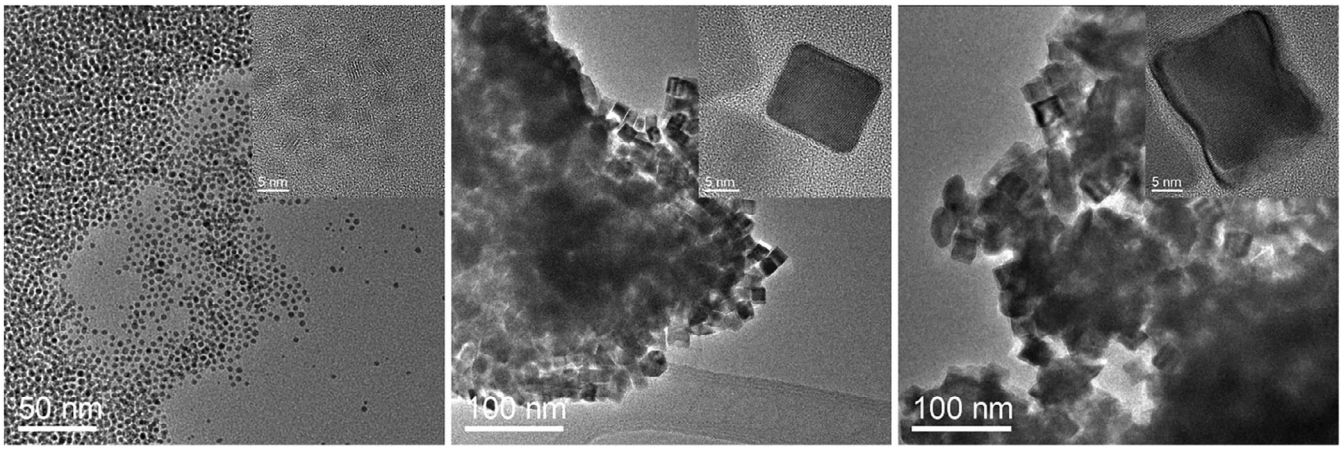

Figure 15. Overview and magnified HRTEM images of larger GSH-coated spherical palladium nanoparticles (5 nm) (**left**), smaller palladium nanocubes (18 nm) (**center**), and larger nanocubes (28 nm) (**right**) after biphasic hydrogenation of **2** with 50 bar hydrogen. Conditions: $n_{substrate}$ = 50 mmol, p_{H2} = 50 bar, $f_{stirrer}$ = 1500 rpm, c_{Pd} = 0.016 mol%, T_{start} = RT, $w_{Pd,H2O}$ = 16 ppm, V_{total} = 60.6 mL, $t_{preforming}$ = 10 min, semibatch conditions.

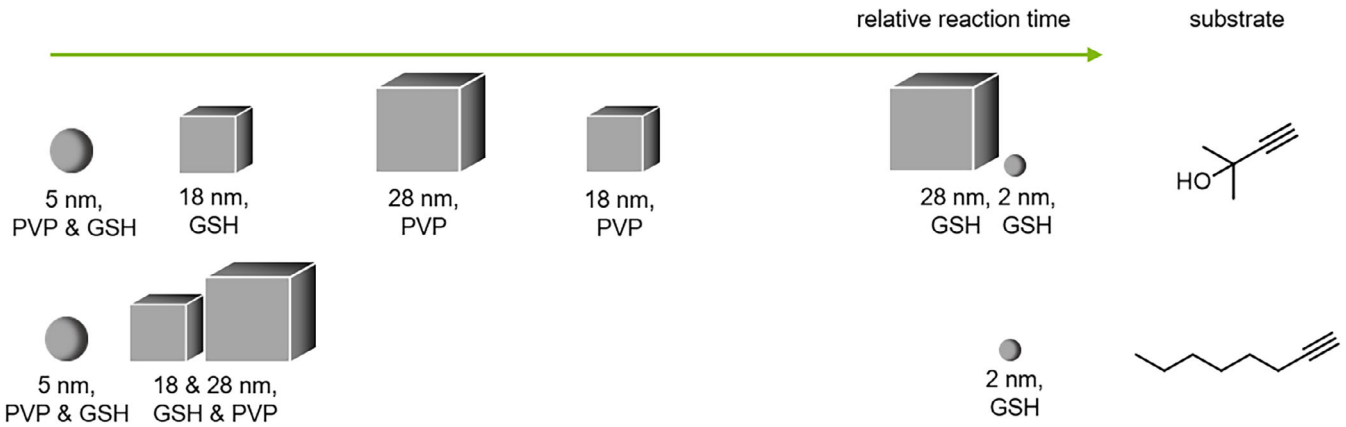

Figure 16. Comparison of the relative reaction times for monophasic (**top row**) and biphasic reactions (**bottom row**).

Table 4. Properties of all nanoparticle catalysts, based on geometrical considerations.

Particle Shape	Mass of One Particle/g	Surface Area of One Particle/m^2	Specific Surface Area of Catalyst/m^2 g^{-1}	Number of Particles in 1 g Catalyst	Number of Palladium Atoms in One Particle[c]	Number of Palladium Atoms on the Surface of One Particle[d]	Number of Palladium Atoms on the Surface in 1 g Catalyst
Spheres (2 nm)[a]	$4.77 \cdot 10^{-20}$	$1.26 \cdot 10^{-17}$	264	$2.10 \cdot 10^{19}$	270	170	$3.54 \cdot 10^{21}$
Spheres (5 nm)[a]	$7.45 \cdot 10^{-19}$	$7.85 \cdot 10^{-17}$	105	$1.34 \cdot 10^{18}$	4200	1260	$1.69 \cdot 10^{21}$
Cubes (18 nm)[b]	$6.64 \cdot 10^{-17}$	$1.94 \cdot 10^{-15}$	29	$1.51 \cdot 10^{16}$	375000	17300	$2.60 \cdot 10^{20}$
Cubes (28 nm)[b]	$2.50 \cdot 10^{-16}$	$4.70 \cdot 10^{-15}$	19	$4.00 \cdot 10^{15}$	1413000	42000	$1.68 \cdot 10^{20}$

[a] The particles were assumed to be perfect spheres with the given diameter.
[b] The particles were assumed to be perfect cubes with the given edge length.
[c] To compute the number of palladium atoms in one particle, the particle volume was divided by the volume of one palladium atom (0.0115 nm^3) and assuming a packing density (fcc) of 74%.
[d] To compute the number of palladium atoms on the surface of spherical particles, a surface layer of 0.28 nm thickness (diameter of one palladium atom) was assumed. The number of palladium atoms in this layer was approximated by dividing it by the volume of one palladium atom and assuming a packing density (fcc) of 74%.

ena inevitably occur, since a certain degree of cross-solubility must be expected, even if small. The nonpolar nature of the substrate leads, upon coordination to the active surface, to a competition with the ligands that otherwise stabilize the particles in water. As the substrate itself is nonpolar, the particles exhibit an increased tendency to disperse in nonpolar media, which results in a destabilization of the aqueous suspension. This effect is further enhanced by the intense stirring required to ensure sufficient mass transfer for high catalytic activity, which additionally enlarges the interfacial area. Our experimental results support this interpretation: Spherical 5 nm particles displayed higher activity, i.e., a more effective substrate coordination and increased turnover, but consequently also a stronger destabilization. In contrast, 2 nm particles showed a lower affinity of the substrate to the surface, resulting in reduced activity but at the same time improved stability. In purely aqueous systems, where the substrate is an alcohol and thus water-soluble, these destabilizing effects are far less pronounced, resulting in a more stable catalytic system overall.

4. Conclusions

Palladium nanoparticles of various sizes and shapes in water, stabilized by either PVP or GSH, are active in the monophasic and biphasic semihydrogenation of alkynes. For biphasic alkyne semihydrogenation, this is the first report of a application of palladium nanoparticles. The ultrasmall nanoparticles had a low efficiency both at 1 and 50 bar hydrogen pressure. The nanoparticles were analyzed before and after the catalytic reaction by electron microscopy to assess possible structural changes. The internal crystallinity of the ultrasmall nanoparticles increased due to reduction by hydrogen but the particles did not agglomerate. In contrast, all larger particles showed a significant aggregation after catalysis but did not significantly change their size and shape.

The semihydrogenation was fast for most particles and never took longer than about 2.5 h to completion. Regarding reaction rates, several trends emerged for both monophasic and biphasic reaction conditions: The ultrasmall particles were always the least efficient with turnover frequencies of 1000–4,000 h^{-1}, while

the 5 nm particles were consistently the most efficient, reaching remarkably high TOFs of up to 183,000 h^{-1}. In biphasic catalysis, mass transport limitations led to similar reaction rates for all larger particles with TOFs around 12,000 h^{-1}. The selectivity was comparable in most cases with about 80%. There was no significant effect of the coating agent (GSH or PVP) on either selectivity or activity in hydrogenation catalysis, indicating that the surface of the palladium nanoparticles is easily accessible in all cases for the substrates.

In monophasic catalysis, most of the palladium could be recovered. In contrast, in biphasic catalysis, a significant palladium loss was found except for the ultrasmall nanoparticles which were fully recovered. In conclusion, nanoparticles with diameter of 5 nm turned out to be most efficient in hydrogenation catalysis. However, the chosen biphasic approach is not suitable for the present catalyst system. Instead, future work should focus on carrying out the reaction in a monophasic aqueous medium (potentially with co-solvents), followed by a downstream separation step such as liquid–liquid extraction.

Acknowledgments

The authors thank the networking program "Sustainable Chemical Synthesis 2.0" (SusChemSys 2.0) for support and fruitful discussions across disciplines. The authors also thank I. Henkel, M. Schwandt and J. Ufer for ICP-OES measurements. N.K. thanks the Konrad-Adenauer-Stiftung for a Ph.D. scholarship.

Open access funding enabled and organized by Projekt DEAL.

Conflict of Interests

The authors declare no conflict of interest.

Data Availability Statement

The data that support the findings of this study are available in the supplementary material of this article.

Keywords: Alkyne hydrogenation · Heterogeneous catalysis · Homogeneous catalysis · Nanoparticles · Palladium

[1] J. W. Arblaster, *Platin Met. Rev.* **2012**, *56*, 181–189.
[2] O. Wetzel, O. Prymak, K. Loza, N. Gumbiowski, M. Heggen, P. Bayer, C. Beuck, C. Weidenthaler, M. Epple, *Inorg. Chem.* **2022**, *61*, 5133–5147.
[3] N. Kost, O. Prymak, K. Loza, M. Heggen, C. Weidenthaler, M. Epple, *Acta Cryst. A* **2024**, *80*, e462.
[4] S. Bhama, T. R. Sibakoti, J. B. Jasinski, F. P. Zamborini, *ChemCatChem* **2020**, *12*, 2253–2261.
[5] M. Perez-Lorenzo, *J. Phys. Chem. Lett.* **2012**, *3*, 167–174.
[6] A. M. Trzeciak, A. W. Augustyniak, *Coord. Chem. Rev.* **2019**, *384*, 1–20.
[7] J. A. Delgado, O. Benkirane, C. Claver, D. Curulla-Ferre, C. Godard, *Dalton Trans.* **2017**, *46*, 12381–12403.
[8] A. Behr, T. Seidensticker, D. Vogt, *Applied Homogeneous Catalysis: A Tool for Sustainable Chemistry*, 2nd ed., Wiley, Newark **2025**.
[9] M. Crespo-Quesada, A. Yarulin, M. Jin, Y. Xia, L. Kiwi-Minsker, *J. Am. Chem. Soc.* **2011**, *133*, 12787–12794.
[10] N. Semagina, A. Renken, D. Laub, L. Kiwi-Minsker, *J. Catal.* **2007**, *246*, 308–314.
[11] J. Chung, C. Kim, H. Jeong, T. Yu, D. H. Binh, J. Jang, J. Lee, B. M. Kim, B. Lim, *Chem. Asian J.* **2013**, *8*, 919–925.
[12] A. Karatzia, Dissertation thesis, University of Duisburg-Essen **2023**.
[13] M. Jin, H. Liu, H. Zhang, Z. Xie, J. Liu, Y. Xia, *Nano Res.* **2011**, *4*, 83–91.
[14] A. Rostek, M. Breisch, K. Pappert, K. Loza, M. Heggen, M. Köller, C. Sengstock, M. Epple, *Beilstein J. Nanotechnol.* **2018**, *9*, 2763–2774.
[15] S. Ermis, K. Kaya, F. Topuz, Y. Yagci, *Inorg. Chem. Commun.* **2023**, *152*, 110626.
[16] J. García-Aguilar, M. Navlani-Garcia, A. Berenguer-Murcia, K. Mori, Y. Kuwahara, H. Yamashita, D. Cazorla-Amoros, *Langmuir* **2016**, *32*, 12110–12118.
[17] R. Narayanan, M. A. El-Sayed, *J. Am. Chem. Soc.* **2003**, *125*, 8340–8347.
[18] Y. Fu, H. Zhang, S. Dai, X. Zhi, J. Zhang, W. Li, *Analyst* **2015**, *140*, 6676–6683.
[19] J. Xian, Q. Hua, Z. Jiang, Y. Ma, W. Huang, *Langmuir* **2012**, *28*, 6736–6741.
[20] G. Clergeaud, R. Genc, M. Ortiz, C. K. O'Sullivan, *Langmuir* **2013**, *29*, 15405–15413.
[21] M. Muniz-Miranda, A. Zoppi, F. Muniz-Miranda, N. Calisi, *Coatings* **2020**, *10*, 207.
[22] S. Sharma, *J. Colloid Interface Sci.* **2015**, *441*, 25–29.
[23] H. Hirai, H. Chawanya, N. Toshima, *Macromol. Chem. Rapid Commun.* **1981**, *2*, 99–103.
[24] A. Yarulin, I. Yuranov, F. Cardenas-Lizana, P. Abdulkin, L. Kiwi-Minsker, *J. Phys. Chem. C* **2013**, *117*, 13424–13434.
[25] A. Behr, H. Schmidke, DE4203351A1, Henkel KGaA, Germany **1993**.
[26] C. W. A. Chan, K. Y. Tam, J. Cookson, P. Bishop, S. C. Tsang, *Catal. Sci. Technol.* **2011**, *1*, 1584.
[27] J. J. Brunet, P. Caubere, *J. Org. Chem.* **1984**, *49*, 4058–4060.
[28] C. Evangelisti, N. Panziera, A. D'Alessio, L. Bertinetti, M. Botavina, G. Vitulli, *J. Catal.* **2010**, *272*, 246–252.
[29] M. M. Telkar, C. V. Rode, R. V. Chaudhari, S. S. Joshi, A. M. Nalawade, *Appl. Catal. A* **2004**, *273*, 11–19.
[30] N. Wolff, C. Beuck, T. Schaller, M. Epple, *Nanoscale Adv.* **2024**, *6*, 3285–3298.
[31] A. Thust, J. Barthel, K. Tillmann, *J. Large-scale Res. Fac.* **2016**, *2*, A41.
[32] N. Gumbiowski, K. Loza, M. Heggen, M. Epple, *Nanoscale Adv.* **2023**, *5*, 2318–2326.
[33] C. A. Schneider, W. S. Rasband, K. W. Eliceiri, *Nat. Meth.* **2012**, *9*, 671–675.
[34] H. Fissan, S. Ristig, H. Kaminski, C. Asbach, M. Epple, *Anal. Meth.* **2014**, *6*, 7324–7334.
[35] M. R. Ibrahim, Z. A. Fataftah, P. von Rague Schleyer, P. D. Stout, *J. Comput. Chem.* **1987**, *8*, 1131–1138.

Manuscript received: July 21, 2025
Revised manuscript received: September 5, 2025
Accepted manuscript online: September 15, 2025
Version of record online: September 24, 2025